Supporting information

Nanoparticulate zero valent iron interaction with dissolved organic matter impacts iron transformation and organic carbon stability

Yanlong Wang[a], Kun Yang[ab], Daohui Lin[*ab]

[a]Department of Environmental Science, Zhejiang University, Hangzhou 310058, China;

[b]Zhejiang Provincial Key Laboratory of Organic Pollution Process and Control, Zhejiang University, Hangzhou 310058, China

*Corresponding author: Tel.: +86 571 88982582; fax: +86 571 88982590.

E-mail address: lindaohui@zju.edu.cn (D. Lin)

Text S1. Synthesis of the CMC coated nZVI ($nZVI_{cmc}$)

Briefly, 30 g/L $nZVI_{20}$ slurry (in 100 mL of 1 mM $NaHCO_3$ solution) were mixed (100 rpm, 25 ± 0.5 °C) with 15 g/L CMC solution (in 50 mL of 1 mM $NaHCO_3$ solution) with pH adjusted to 9.5 by NaOH. After 72 h of mixing by magnetic stirring, the surface coated $nZVI_{20}$ was separated by centrifugation and was then freeze-dried.

Text S2. Analysis conditions of high performance size exclusion chromatography (HPSEC)

Ultrapure water and acetonitrile (80% : 20%) with 0.1 M NaCl were used as the mobile phase with a flow rate maintained at 1.0 mL/min. Before use, the mobile phase was vacuum-filtered through a 0.45-μm membrane filter using an all-glass filtration apparatus. Sodium polystyrenesulfonate with different MWs were used as SEC MW standards. All standards and samples were measured at a detection wavelength of 254 nm. A calibration curve was constructed based on the linear relationship between the retention time corresponding to the highest peak and the lgMW. DOM MW values were determined from the chromatograms using the calibration equation.

Text S3. Fluorescence intensity integration

According to previous studies[1, 2], different types of organics have different excitation–emission wavelengths and the 3D EEM spectra can be divided into five regions: region I is related to tyrosine-like protein (Ex 200–250 nm, Em 250–330 nm), region II to tryptophan-like protein (Ex 200–250 nm, Em 330–380 nm), region III to fulvic acid-like organics (Ex 200–250 nm, Em 380–650 nm), region IV to soluble microbial by-product-like materials (Ex 250–450 nm, Em 250–380 nm), and region V to humic acid-like organics (Ex 250–450 nm, Em 380–650 nm). By the deduction of the cumulative excitation–emission area in the blank, the fluorescence intensity integration for each region i ($\Phi_{i,n}$) was calculated with Eq. (1) [1, 2]

$$\emptyset_{i,n} = \sum ex \sum emI(\lambda_{ex}\lambda_{em})\Delta\,\lambda_{ex}\Delta\lambda_{em} \quad (1)$$

where I ($\lambda_{ex}\lambda_{em}$) is the fluorescence intensity at each excitation–emission wavelength pair; $\Delta\lambda_{ex}$ and $\Delta\lambda_{em}$ are the excitation and emission wavelength increments (10 nm), respectively.

Table S1 FTIR peak assignments for DOM and nZVIs-adsorbed DOM

Band number	Peak position (cm^{-1})				Assignments	Reference
	HA	HA-nZVIs	FA	FA-nZVIs		
Band 1	2923	2923	2932	2921	Asymmetric CH stretching in $–CH_3$ and $–CH_2–$ of aliphatic chains	[3]
Band 2	2854	2841	2841	2850	Symmetry CH stretching in $–CH_3$ and $–CH_2–$ of aliphatic chains	[3]
Band 3	-	-	1709	-	Protonated carboxylic C=O stretching	[4,5-7]
Band 4	1586	1620	1587	1620	Aromatic C=C functional groups	[6-9]
Band 5	1384	1381	-	1378	Symmetrical stretching of carboxyl functional groups complexed with iron	[7, 9]
Band 6			1514	Disappeared	Aromatic C=C stretching and/or N-H deformation	[10, 11]
Band 7			1463	Disappeared	C-H deformations in CH_2 and CH_3 groups	[10, 11]
Band 8			1423	Disappeared	C=O stretching vibrations	[10, 11]
Band 9			1330	Disappeared	C–H deformation	[11, 12]

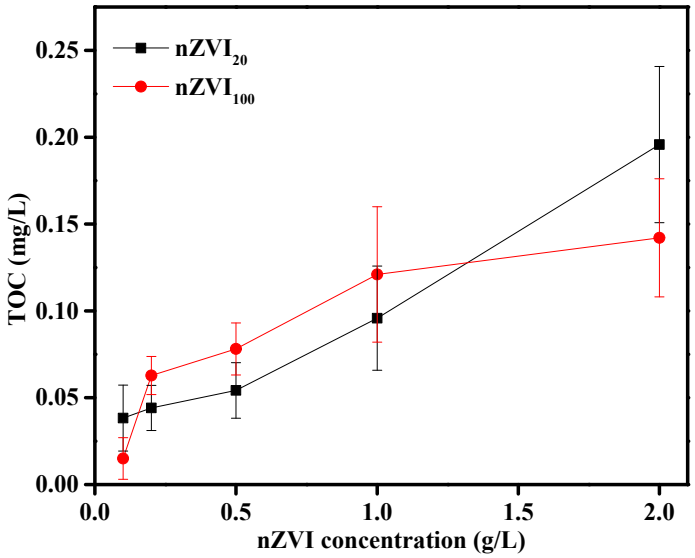

Fig. S1 Total organic carbon (TOC) desorbed from different concentrations of bare nZVIs in the background solution (0.01 M NaCl) after equilibration for 48 h.

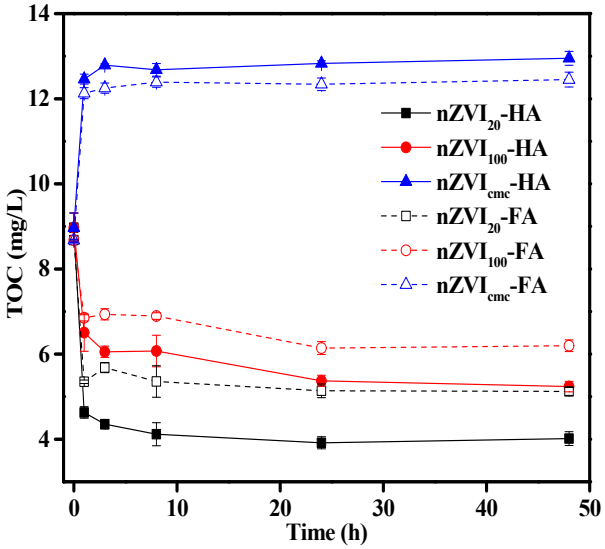

Fig. S2 Time-dependent changes in TOC content of DOM solutions (25 mg/L) by treatment with different nZVIs for various time (1 g/L NPs, 0.01 M NaCl, pH = 6.5 ± 0.5, and T = 298 K).

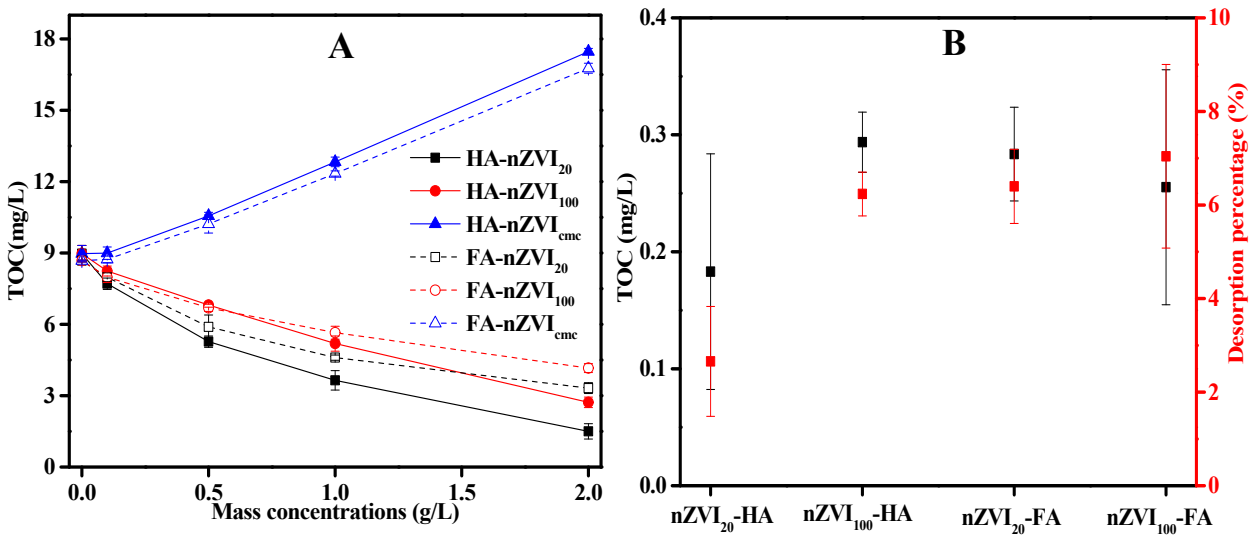

Fig. S3 (A) Changes in TOC content of DOM solutions (25 mg/L) against the 48 h adsorption by different concentrations of nZVIs; (B) desorbed TOC concentrations and the desorption percentages of nZVIs-adsorbed DOM after the desorption for 48 h in 0.01 M NaCl solutions (pH = 6.5 ±0.5 and T = 298 K).

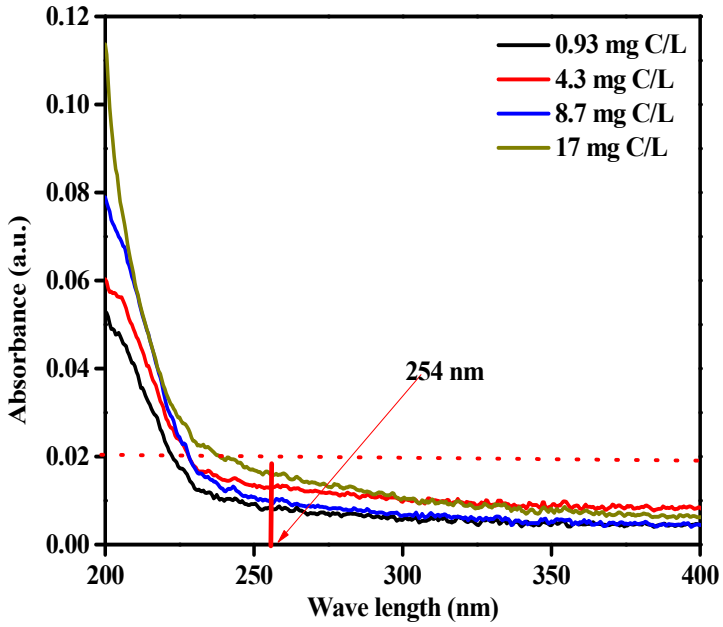

Fig. S4 Ultraviolet absorption spectra of different concentrations of CMC solutions.

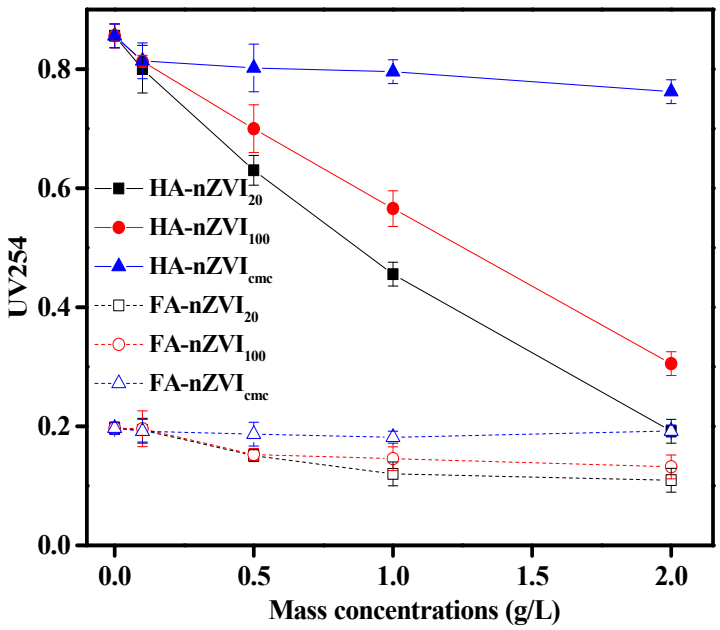

Fig. S5 Changes in UV254 of DOM solutions (25 mg/L) against the 48 h adsorption by various concentrations of nZVIs (0.01 M NaCl, pH = 6.5 ± 0.5, and T = 298 K).

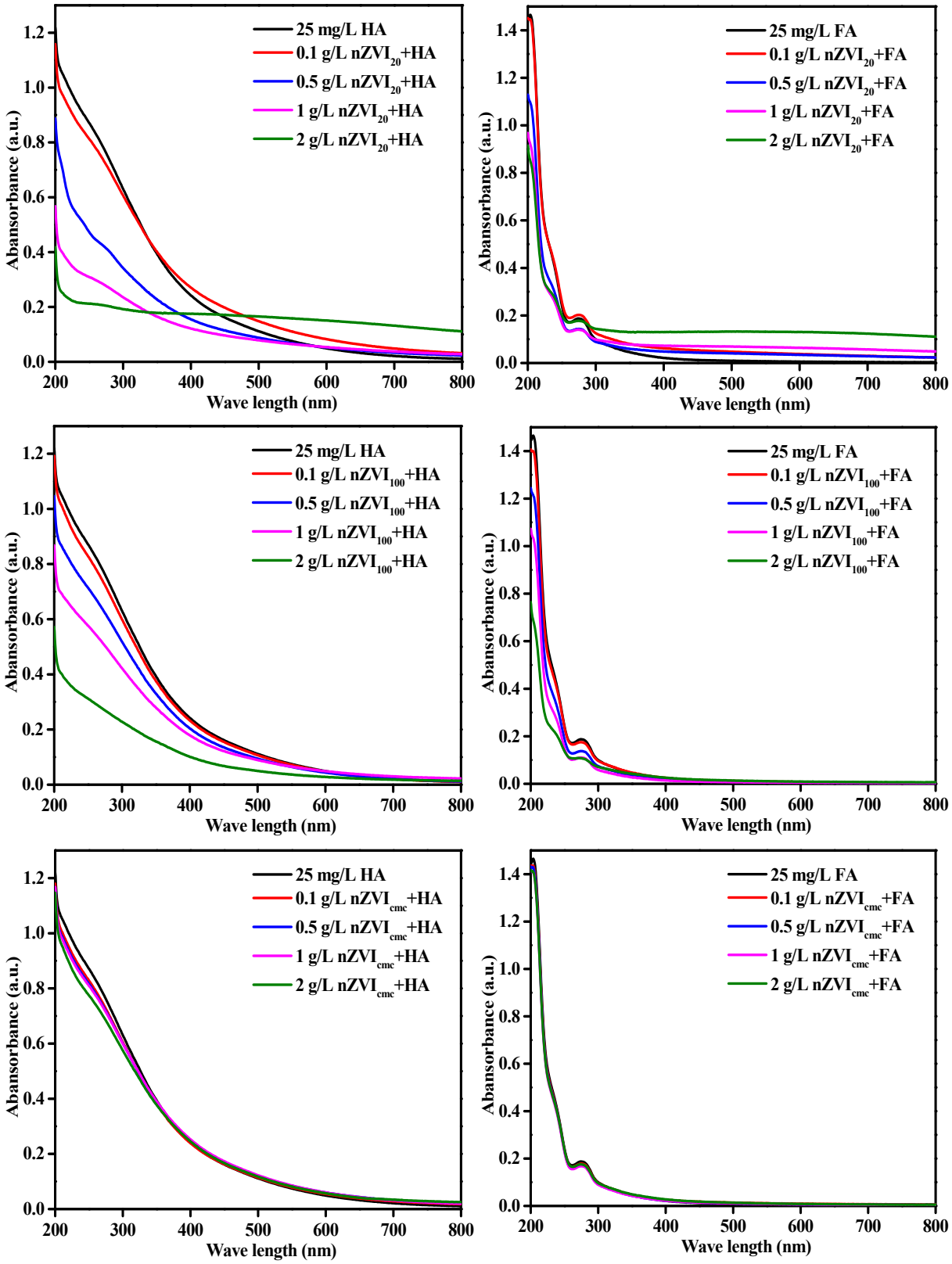

Fig. S6 Ultraviolet-visible absorbance spectra of DOM solutions before and after the treatment with different concentrations of nZVIs. Conditions: 0.01 M NaCl, pH = 6.5 ± 0.5, T = 298 K, and 48 h adsorption.

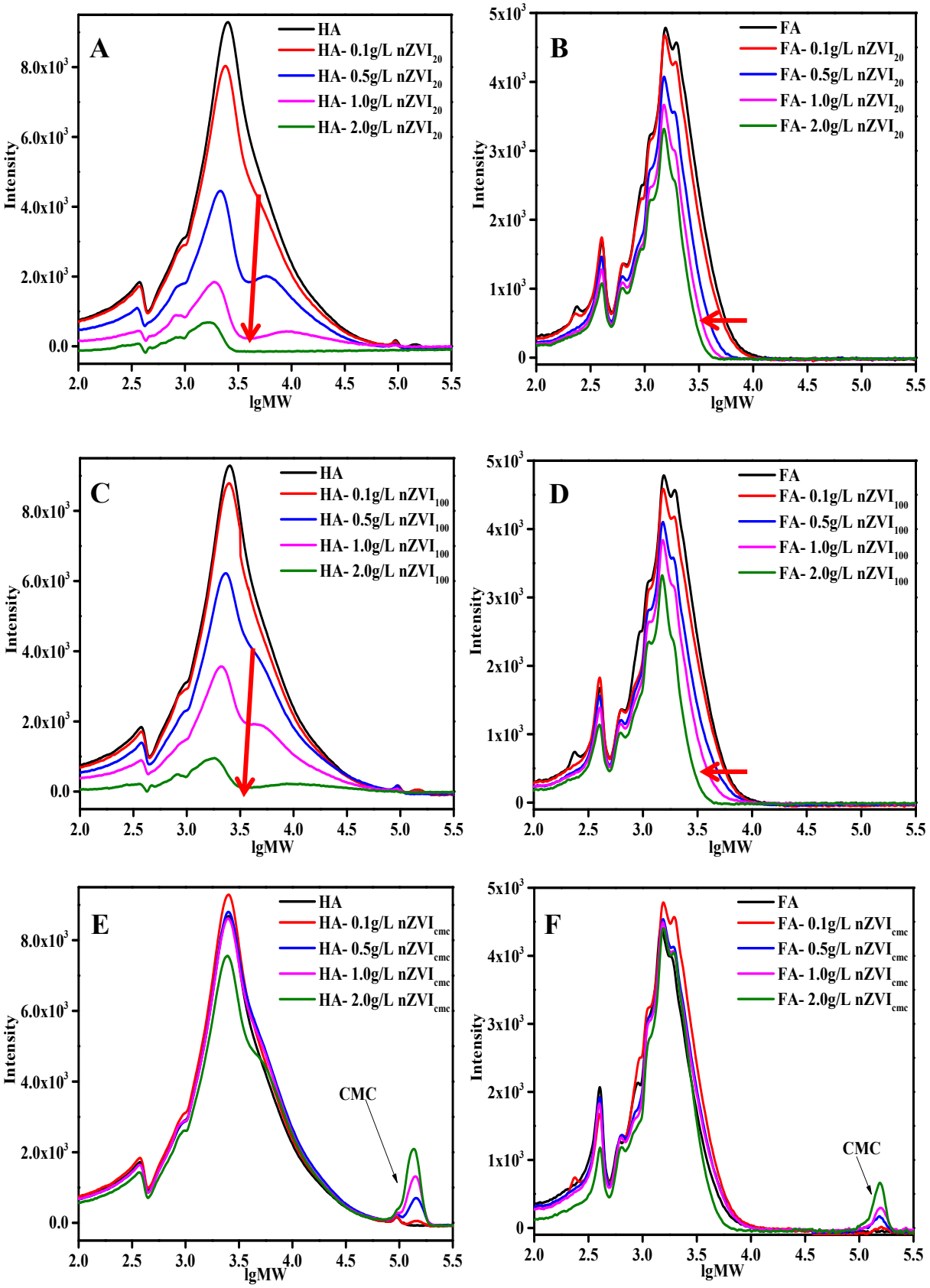

Fig. S7 Molecular weight distributions of DOM solutions before and after the treatment with nZVIs at different concentrations (25 mg/L DOM, 0.01 M NaCl, T = 298 K, and 48 h adsorption).

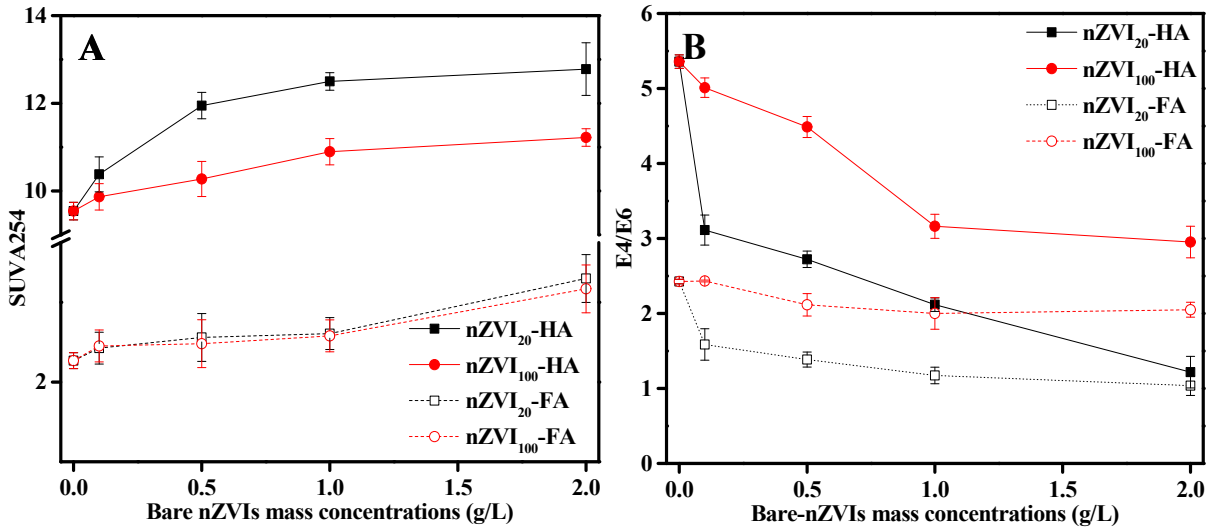

Fig. S8 Changes in SUVA254 (A) and E4/E6 (B) of DOM against the 48 h adsorption by nZVIs at different concentrations (25 mg/L DOM, 0.01 M NaCl, pH=6.8 ±0.5, and T=298 K).

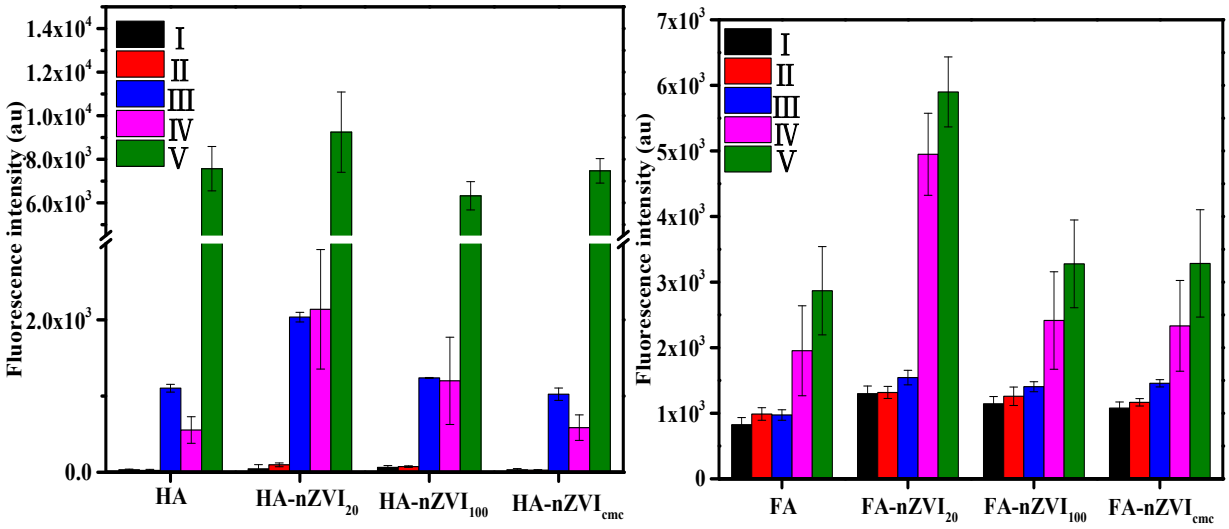

Fig. S9 Fluorescence intensity integration for each 3D EEM region of DOM solutions before and after the 48-h adsorption by nZVIs. Conditions: 2 g/L nZVIs, 25 mg/L DOM, 0.01 M NaCl, and T = 298 K.

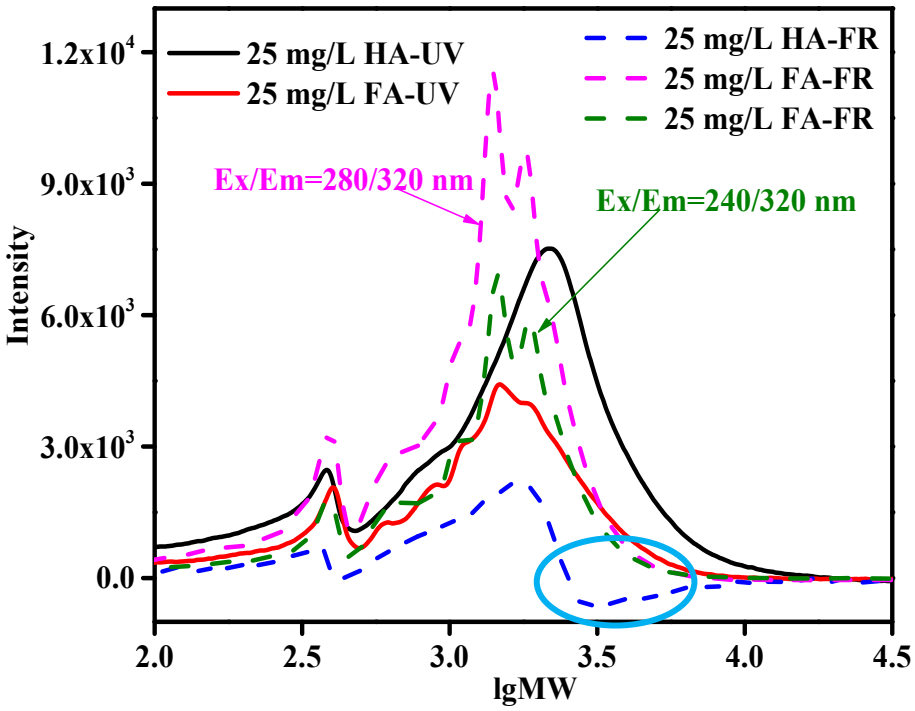

Fig. S10 Molecular weight distributions of DOM solutions detected by UV and fluorescence (FR) detectors.

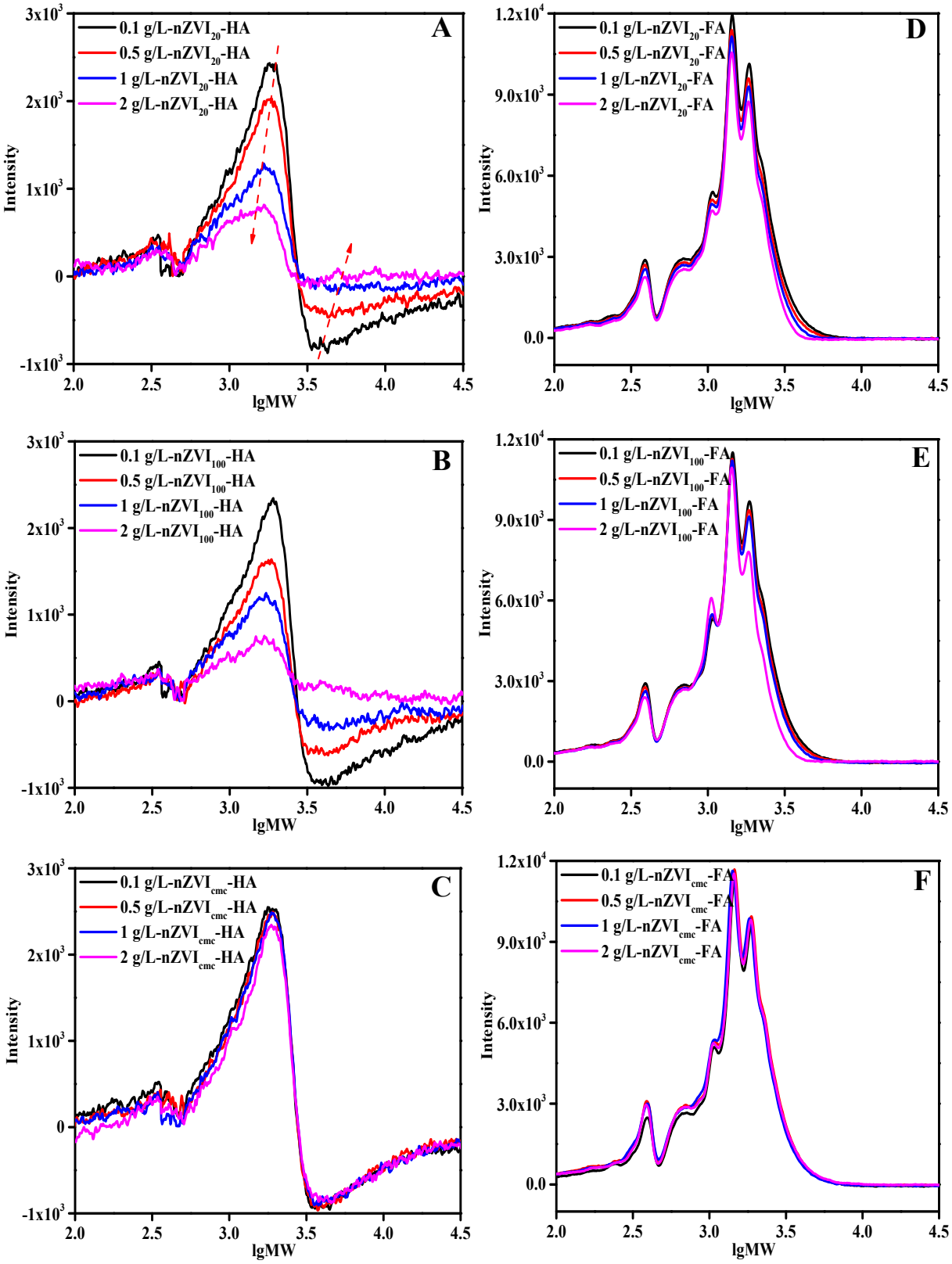

Fig. S11 Changes in MW distributions of DOM fluorophores against the 48 h adsorption of nZVIs at different concentrations (25 mg/L DOM, 0.01 M NaCl, pH=6.8 ±0.5, and T=298 K).

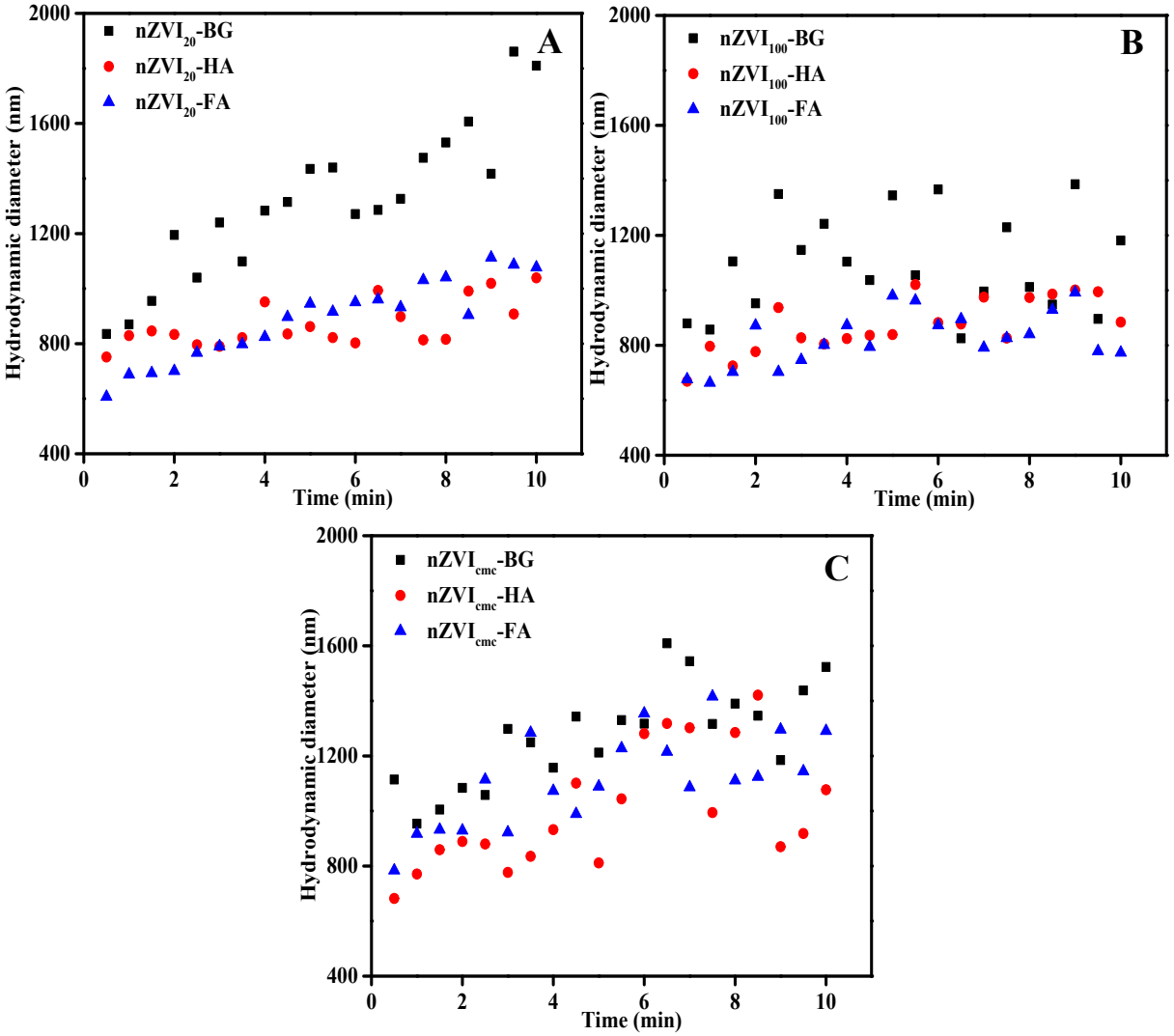

Fig. S12 Time-dependent variations in hydrodynamic diameters of 200 mg/L nZVIs in background (BG) and DOM solutions (25 mg/L DOM, 0.01 M NaCl, pH = 6.5 ± 0.5, and T = 298 K).

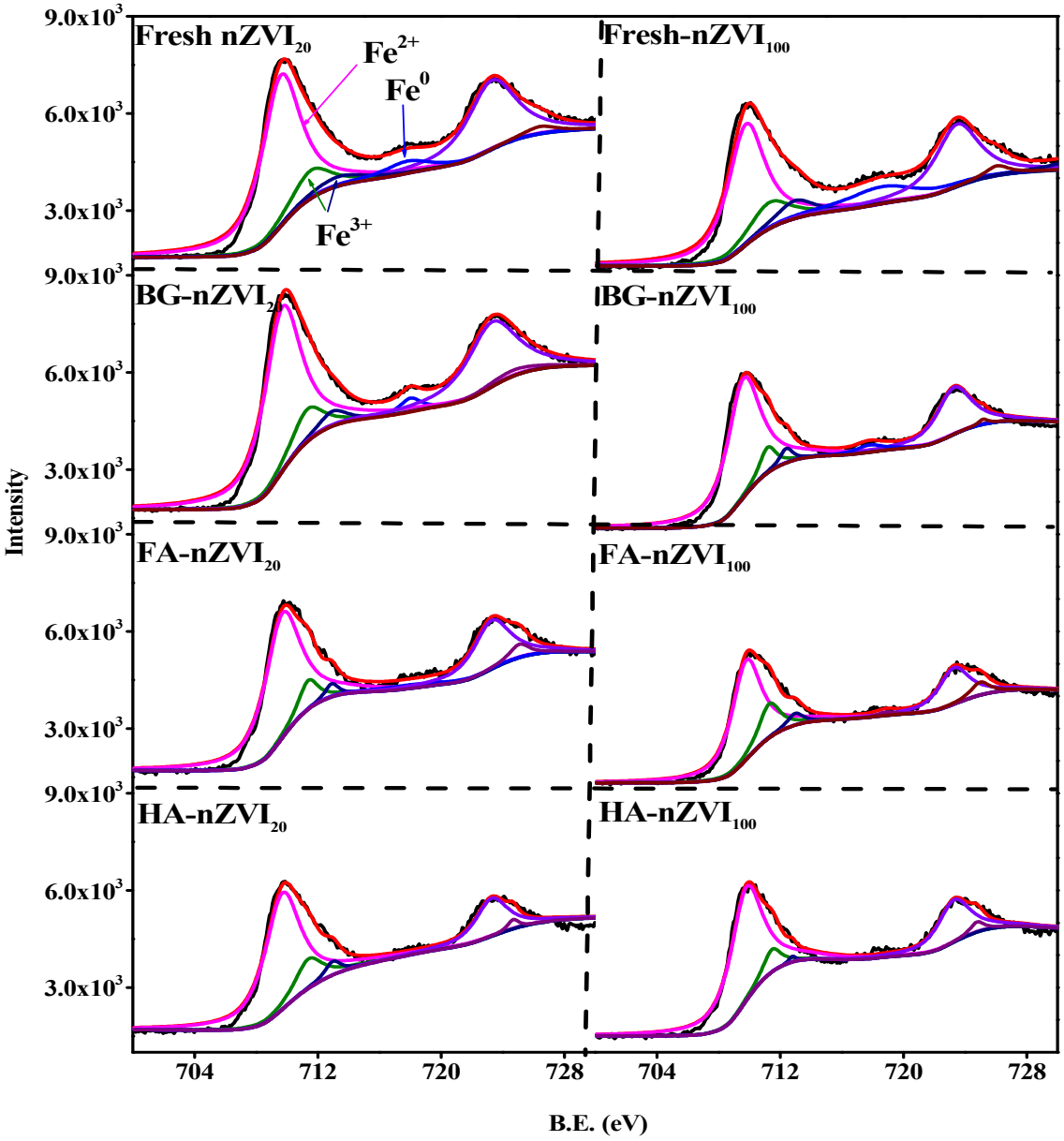

Fig. S13 XPS spectra of Fe 2p in nZVIs before (fresh) and after the aging in the background solution (BG) or DOM solutions for 48 h. The peak located at around 709.5 eV is ascribed to the binding energies of Fe $2p_{3/2}$ orbital from Fe^{2+} in Fe_3O_4, the peaks around 711.6 eV and 713.3 eV are assigned to the binding energies of $2p_{3/2}$ of Fe^{3+} in Fe_2O_3/Fe_3O_4, and the shoulder at 719.6 eV is associated with Fe $2p_{1/2}$ orbital in Fe^0[13-16]. The black lines are the measured XPS spectra and the red lines are the fits.

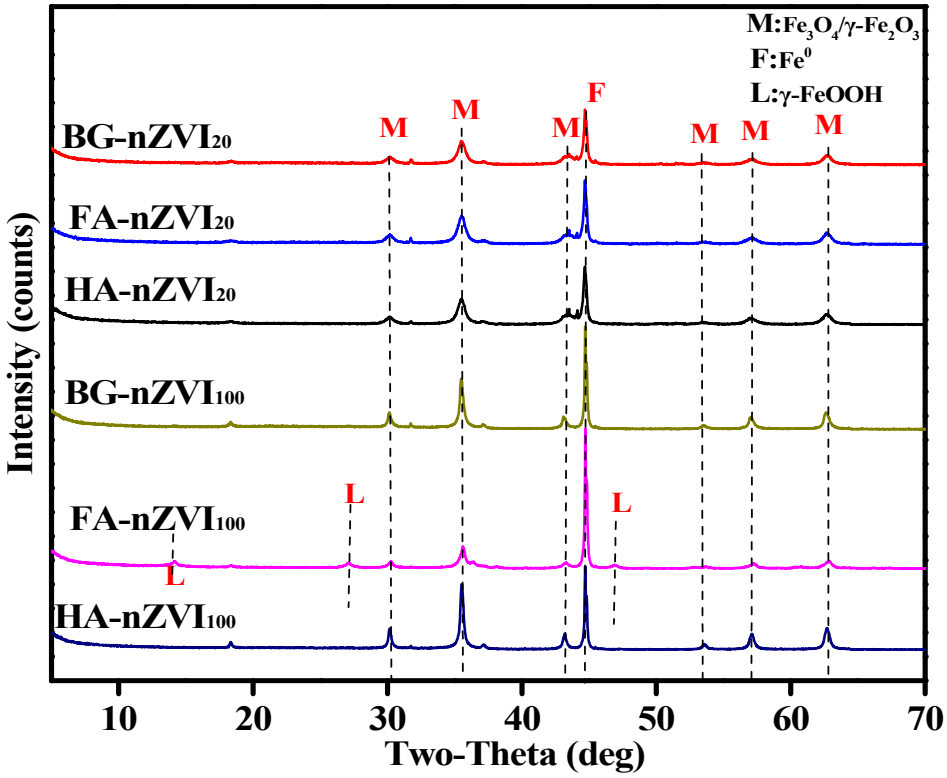

Fig. S14 XRD spectra of nZVIs oxidizing in different solutions (8 days). BG represents the background solution (10 mM NaCl in ultrapure water).

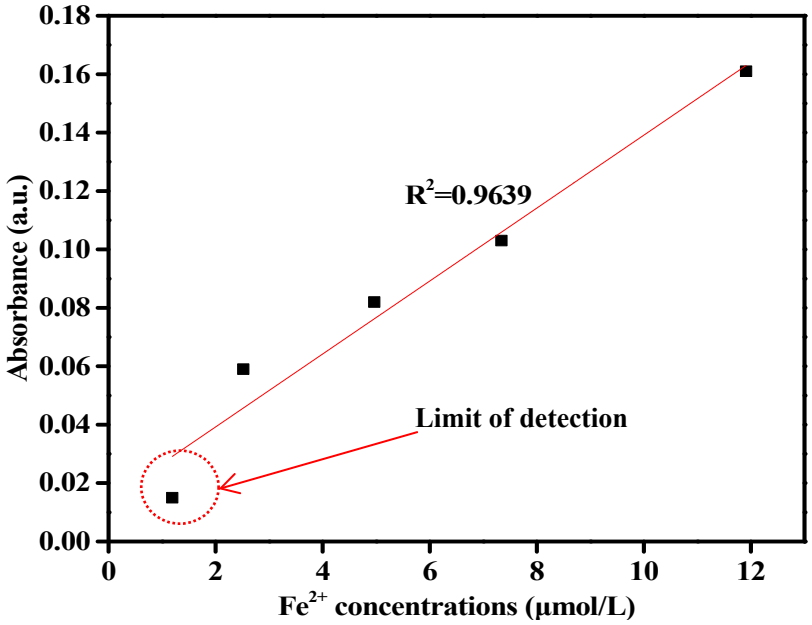

Fig. S15 Calibration curves between the absorbance at 512 nm and Fe^{2+} concentrations.

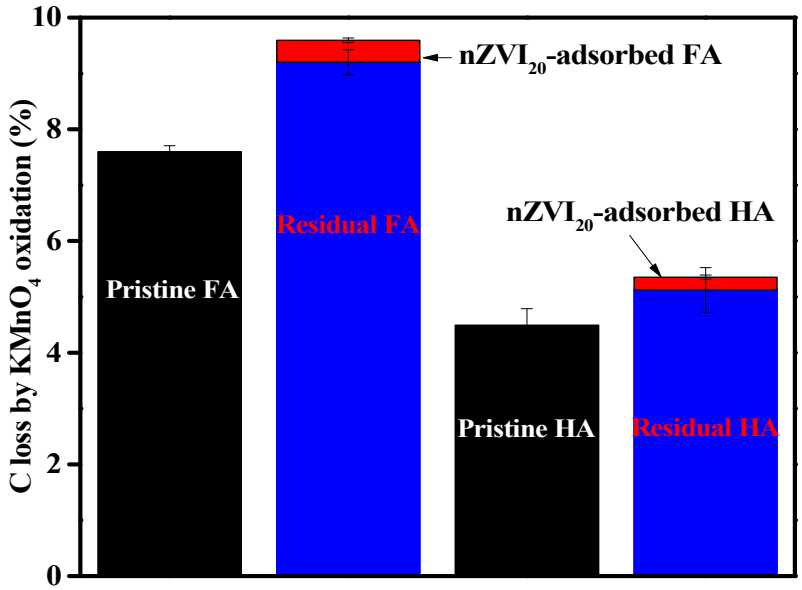

Fig. S16 Carbon loss percentages of the pristine DOM (25 mg/L) upon the $KMnO_4$ (33 mM) oxidation and the ratios of organic carbon loss in the residual DOM and nZVI-adsorbed DOM to the total organic carbon of pristine DOM.

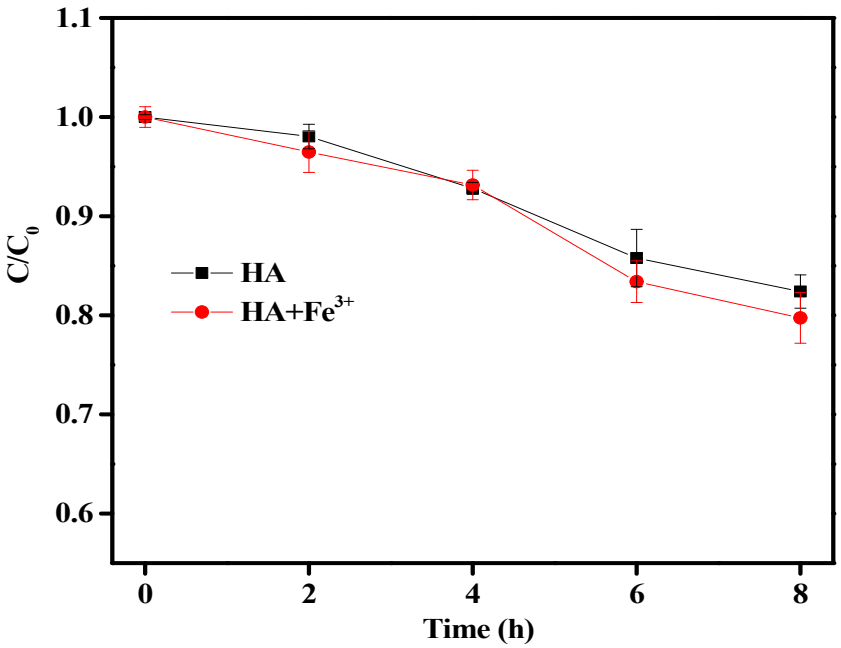

Fig. S17 Changes in the TOC content of HA solution (25 mg/L) against the UV irradiation time with or without 100 μmol/L $Fe(NO_3)_3$.

References cited

(1) Chen, W., Westerhoff, P., Leenheer, J.A., Booksh, K., 2015, Fluorescence excitation−emission matrix regional integration to quantify spectra for dissolved organic matter. Environmental Science & Technology 37(24), 5701-5710.

(2) Guo, L., Lu, M.M., Li, Q.Q., Zhang, J.W., She, Z.L., 2015, A comparison of different pretreatments on hydrogen fermentation from waste sludge by fluorescence excitation-emission matrix with regional integration analysis. International Journal of Hydrogen Energy 40(1), 197-208.

(3) Fukushima, M., Tatsumi, K., Nagao, S., 2001, Degradation characteristics of humic acid during photo-Fenton processes. Environmental Science & Technology 35(18), 3683-3690.

(4) Zaccheo, P., Cabassi, G., Ricca, G., Crippa, L., 2002, Decomposition of organic residues in soil: experimental technique and spectroscopic approach. Organic Geochemistry 33(3), 327-345.

(5) Karlsson, T., Persson, P., 2012, Complexes with aquatic organic matter suppress hydrolysis and precipitation of Fe(III). Chemical Geology 322, 19-27.

(6) Eusterhues, K., Rennert, T., Knicker, H., Kogel-Knabner, I., Totsche, K.U., Schwertmann, U., 2011, Fractionation of organic matter due to reaction with ferrihydrite: coprecipitation versus adsorption. Environmental Science & Technology 45(2), 527-533.

(7) Gu, B.H., Schmitt, J., Chen, Z., Liang, L.Y., McCarthy, J.F., 1995, Adsorption and desorption of different organic-matter fractions on iron-oxide. Geochimica Et Cosmochimica Acta 59(2), 219-229.

(8) Chen, C., Dynes, J.J., Wang, J., Sparks, D.L., 2014, Properties of fe-organic matter associations via coprecipitation versus adsorption. Environmental Science & Technology 48(23), 13751-13759.

(9) Sowers, T.D., Stuckey, J.W., Sparks, D.L., 2018, The synergistic effect of calcium on organic carbon sequestration to ferrihydrite. Geochemical Transactions 19, 4.

(10) Eusterhues, K., Rennert, T., Knicker, H., Kogel-Knabner, I., Totsche, K.U., Schwertmann, U., 2011, Fractionation of organic matter due to reaction with ferrihydrite: coprecipitation versus adsorption. Environmental Science & Technology 45(2), 527-533.

(11) Pandey, K.K., Pitman, A.J., 2003, FTIR studies of the changes in wood chemistry following decay by brown-rot and white-rot fungi. International Biodeterioration & Biodegradation 52(3), 151-160.

(12) Richard, C., Guyot, G., Rivaton, A., Trubetskaya, O., Trubetskoj, O., Cavani, L., Ciavatta, C., 2007, Spectroscopic approach for elucidation of structural peculiarities of andisol soil humic acid fractionated by SEC-PAGE setup. Geoderma 142(1-2), 210-216.

(13) Li, H., Chen, S., Ren, L.Y., Zhou, L.Y., Tan, X.J., Zhu, Y., Belver, C., Bedia, J., Yang, J., 2019, Biochar mediates activation of aged nanoscale zvi by shewanella putrefaciens cn32 to enhance the degradation of pentachlorophenol. Chemical Engineering Journal 368, 148-156.

(14) Liu, X., Cao, Z., Yuan, Z., Zhang, J., Guo, X., Yang, Y., He, F., Zhao, Y., Xu, J., 2018, Insight into the kinetics and mechanism of removal of aqueous chlorinated nitroaromatic antibiotic chloramphenicol by nanoscale zero-valent iron. Chemical Engineering Journal 334, 508-518.

(15) Lyu, H., Tang, J., Huang, Y., Gai, L., Zeng, E.Y., Liber, K., Gong, Y., 2017, Removal of hexavalent chromium from aqueous solutions by a novel biochar supported nanoscale iron sulfide composite. Chemical Engineering Journal 322, 516-524.

(16) Mortazavian, S., An, H., Chun, D., Moon, J., 2018, Activated carbon impregnated by zero-valent iron nanoparticles (AC/nZVI) optimized for simultaneous adsorption and reduction of aqueous hexavalent chromium: material characterizations and kinetic studies. Chemical Engineering Journal 353, 781-795.